Active Control of Combustion Instabilities in Gas Turbine Engines for Low Emissions. Part I: Physics-Based and Experimentally Identified Models of Combustion Instability

C.A. Jacobson
United Technologies Research Center,
MS129-15, 411 Silver Lane, East Hartford, CT 06108, USA
tel. 860 610 7652, **jacobsca@utrc.utc.com**

A.I. Khibnik
United Technologies Research Center,
MS129-15, 411 Silver Lane, East Hartford, CT 06108, USA
tel. 860 610 7403, **khibniai@utrc.utc.com**

A. Banaszuk
United Technologies Research Center,
MS129-15, 411 Silver Lane, East Hartford, CT 06108, USA
tel. 860 610 7381, **banasza@utrc.utc.com**

J. Cohen
United Technologies Research Center,
MS129-16, 411 Silver Lane, East Hartford, CT 06108, USA
tel. 860 610 7973, **cohenjm@utrc.utc.com**

W. Proscia
United Technologies Research Center,
MS129-16, 411 Silver Lane, East Hartford, CT 06108, USA
tel. 860 610 7679, **prosciw@utrc.utc.com**

May 2000

Abstract

This paper details the development of a thermoacoustic model and associated dynamic analysis. The model describes the results obtained in a gas fueled experimental combustion program carried out at UTRC.

The contents of the paper are (a) the development of a thermoacoustic model composed of acoustic and heat release components, (b) the dynamic analysis of the resulting nonlinear model using harmonic balance methods to compute linear stability boundaries and the amplitudes of oscillations and (c) the calibration of the model to experimental data.

1 Introduction

This paper presents a thermoacoustic model structure for describing the dynamics associated with lean premixed combustion instabilities. The model developed is used to describe the dynamics of a single nozzle rig (SNR) experimental program carried out at UTRC. This paper also contains analysis of this model for both linear stability boundaries as well as amplitudes of oscillations subsequent to the loss of linear stability. The calibration of model parameters using experimentally measured data is also included. The purpose of the modeling effort is to obtain a calibrated model of the single-nozzle combustor that can be used to analyze the effects of closed loop control, and most importantly, to ultimately predict the control authority needed to reduce the amplitude of the pressure oscillations to an acceptable level. This paper represents a contribution from a continuing program at UTRC that develops combustion dynamics and control from a set of scaled experiments where the scaled experiments are carefully constructed to capture the behavior of full scale engine dynamics and, importantly, the scaled experiments may be reflected back to gain insight into the governing phenomena under investigation.

The results presented in the current work both complement as well as extend related research efforts in obtain-

Paper presented at the RTO AVT Symposium on "Active Control Technology for Enhanced Performance Operational Capabilities of Military Aircraft, Land Vehicles and Sea Vehicles", held in Braunschweig, Germany, 8-11 May 2000, and published in RTO MP-051.

ing reduced order models of combustion instabilities. The works of [5, 7, 8, 11] are of particular interest. The papers [5, 7] concern the development of coupled acoustic-heat release models where the heat release models are focused on unsteady flame dynamics. The work of [11] is more closely related to the current paper where the heat release model is focused on unsteady equivalence ratio variations. This is also true of the work of [6] which models afterburner instabilities that are driven by fluctuating equivalence ratio, however, the coupling to the acoustics is different in that work from the current paper.

The contribution of this paper is to develop a thermoacoustic model that describes the single-nozzle combustor experimental results. The methodology developed here consists of describing the physics based model components and then performing analysis and calibration using this framework. The model framework consists of a feedback interconnection of an acoustic component driven by a heat release component. The nature of the feedback is as follows. The fluctuating heat release component is dependent on the fluctuating equivalence ratio at a flame sheet a distance away from the nozzle exit, and, as it is assumed that the fuel flow rate is constant the fluctuating equivalence ratio is thus dependent on the fluctuating velocity at the nozzle exit which closes the feedback loop. The spatial distance of the flame sheet from the nozzle exit can be viewed as a temporal time delay (convective lag) of the nozzle velocity to create a variation in equivalence ratio and hence the structure of the resulting model is a nonlinear delay differential equation.

The resulting model of the combustion instability is then analyzed using harmonic balance methods to compute linear stability boundaries and amplitudes of oscillation. The model contains an empirical gain factor and the paper develops a methodology to calibrate the model to experimental data using dynamic and stochastic analysis tools. The metrics for this calibration are (a) to match the trend in amplitude as a function of mean equivalence ratio, (b) to match the frequencies of oscillation and (c) to match the power spectral densities and probability function distributions of the measured pressure time traces.

The organization of this paper is as follows. Section 2 presents the modeling framework. This includes both the modeling of the acoustics as well as the heat release in the combustor. Section 3 presents analysis of the model that gives some qualitative insight into the structure of the dynamic behavior with special attention to the self-excited oscillatory behavior. Section 4 presents the calibration procedure that has been used to date. Section 5 summarizes the structure of the models, the methodology that has been developed, the results from this investigation and finally the enumeration of major remaining items of investigation.

2 Thermoacoustic Model Structure

This section presents the basic structure of the thermoacoustic model for single nozzle rig (SNR). The model is composed as a feedback interconnection of acoustic and heat release submodels. The physical single nozzle rig is shown in Figure 1. The subsections below divide the modeling into acoustic considerations and heat release considerations.

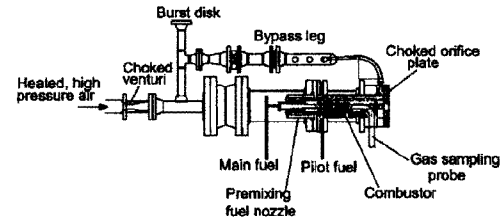

Figure 1: Single Nozzle Rig Used in Experimental Study

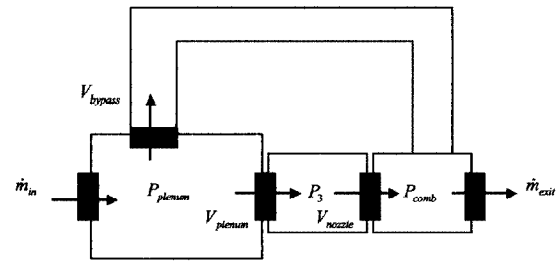

Figure 2: Schematic for Acoustic Modeling

2.1 Acoustic Component

The schematic representation used for modeling the single nozzle rig is depicted in Figure 2. The modeling of this schematic by a set of coupled ordinary differential equations can be done using momentum and mass conservation equations for flow through the orifices and volumes. Choking of the exit orifice is clearly applicable as the combustor pressure is roughly 220 psia and the pressure in the exhaust is roughly 20 psia. The boundary condition at the choked inlet venturi is taken to be a fixed mass flow rate. The equations for this description are as follows. Details may be found in [15] for the orifice relation and [4] for the volume and choked orifice conditions.

$$
\begin{aligned}
\dot{m}_{exit} &= \frac{\kappa C_d A_e P_{comb}}{\sqrt{T_4}} \\
C_{comb}\frac{dP_{comb}}{dt} &= \dot{m}_{nozzle} + \dot{m}_{bypass} \\
&\quad -\dot{m}_{exit} + F \\
\dot{m}_{nozzle} &= \rho_3 A_{nozzle} V_{nozzle} \\
\dot{m}_{bypass} &= \rho_3 A_{bypass} V_{bypass} \\
\rho_3 L_{nozzle}\frac{dV_{nozzle}}{dt} &= -\frac{\rho_3}{2} k_{nozzle} V_{nozzle}^2 \\
&\quad +P_{pre} - P_{comb} \\
C_{pre}\frac{dP_{pre}}{dt} &= \dot{m}_{perf} - \dot{m}_{nozzle} \\
\dot{m}_{perf} &= \rho_3 A_{perf} V_{perf} \\
\rho_3 L_{perf}\frac{dV_{perf}}{dt} &= -\frac{\rho_3}{2} k_{perf} V_{perf}^2 \\
&\quad +P_{plenum} - P_{pre} \\
C_{plenum}\frac{dP_{plenum}}{dt} &= \dot{m}_{in} - \dot{m}_{bypass} - \dot{m}_{perf} \\
\rho_3 L_{bypass}\frac{dV_{bypass}}{dt} &= -\frac{\rho_3}{2} k_{bypass} V_{bypass}^2 \\
&\quad +P_{plenum} - P_{comb}
\end{aligned} \tag{1}
$$

The parameters are described in Table 1.

The resulting model is a nonlinear differential equation where the nonlinearity occurs in the unsteady momentum equation.

The calibration of the model from the mean values of the pressure drops and the air velocity, using mean flow rates and cold flow (nonreacting) experimental data, is as follows. The issue is to choose the effective flow areas ($C_d A$) of the orifices, particularly, the nozzle and the bypass leg. We can use analytical formulas for steady states to guide this choice. Steady state values for pressures and velocities across the system can be computed using the equations alone:

$$
\begin{aligned}
V^s_{nozzle} &= \frac{\dot{m}_{in}}{\rho_3(A_{bypass}\delta + A_{nozzle})} \\
V^s_{bypass} &= \delta V^s_{nozzle} \\
V^s_{perf} &= \frac{A_{nozzle}}{A_{perf}} V^s_{nozzle} \\
P^s_{comb} &= \frac{\sqrt{T_4}}{\kappa C_d A_e}(\dot{m}_{in} V^s_{nozzle}) \\
P^s_{pre} &= P_{comb} + \frac{\rho_3 k_{perf}}{2}(V^s_{nozzle})^2 \\
P^s_{plenum} &= P^s_{pre} + \frac{\rho_3 k_{perf}}{2}(V^s_{perf})^2
\end{aligned} \tag{2}
$$

where

$$
\delta = \left(\frac{k_{nozzle} + k_{perf}\left(\frac{A_{nozzle}}{A_{perf}}\right)^2}{k_{bypass}} \right)^{1/2}
$$

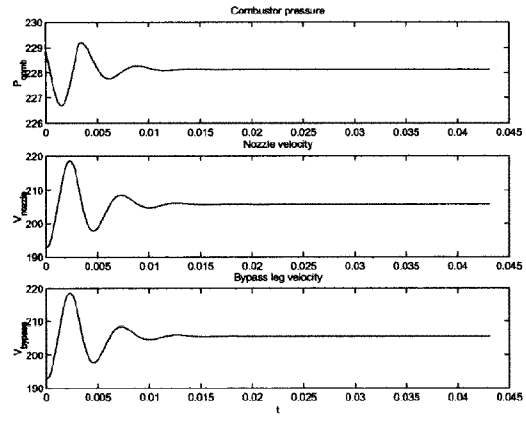

Figure 3: Combustor pressure, nozzle velocity and bypass leg velocity with no combustion

The physical area, A_{nozzle}, and the effective flow area, $C_d A$, for the nozzle have been measured. The length coefficients (L_{nozzle}, etc) are taken as physical parameters for the physical length (but also could be fit to experimentally measured admittance data for the nozzle used in single nozzle rig tests). The bypass leg parameters are set similarly. The discharge coefficient (C_d) for the bypass leg is taken as 0.7, a typical value for a sharp edge orifice. The physical area A_{bypass} is adjusted so that 21% of the flow is through the bypass leg. Again, the physical length of the orifice is taken for L_{bypass}. This sets all parameters for the acoustics. The final choice of parameters for the model is given in Table 2. The steady state values for these parameters using (2) are $P_{comb} = 228.15, P_{pre} = 233.56, P_{plenum} = 242.07, V_{nozzle} = 205.69, V_{perf} = 283.86, V_{bypass} = 282.86$.

Calibration procedure can also include mean flow rates and cold flow (nonreacting) experimental data. Specifically the mass flow rates (in lbm/sec) predicted by the model can be compared to design values for the combustor. The design value of mass flow rate is 6.2 lbm/sec for the single nozzle rig which compares with the mass flow rate (through the nozzle) as 5.15 in the model after calibration. The pressure drop across the nozzle was calculated as 2.4%.

A simulation of the equations of motion with parameter values in table 2 produces the velocity and pressure plots shown in Figure 3. The initial conditions were chosen to be off steady state to reveal a heavily damped system.

2.2 Heat Release Component

This section outlines the modeling of the heat release subsystem as a velocity sensitive mechanism.

The addition of a heat release component to the acoustic component considered above can proceed from the equation for mass conservation as in [10]. The equation is

$$
\frac{\partial \rho}{\partial t} + \nabla \cdot (\rho U) = 0
$$

where U is the air velocity and ρ the density. The density is represented as a function of pressure P and entropy S, $\rho = \rho(P, S)$. Then

$$\frac{\partial \rho}{\partial t} = \left(\frac{\partial \rho}{\partial P}\right)_S \frac{\partial P}{\partial t} + \left(\frac{\partial \rho}{\partial S}\right)_P \frac{\partial S}{\partial t}$$

Then [10] the first term can be expressed in terms of the local sound speed and noting that

$$\left(\frac{\partial \rho}{\partial S}\right)_S = -\frac{\rho}{c_P}$$

with c_P the specific heat per unit mass at constant pressure. In addition if there is a continuous volume distribution of heat release at a rate of q per unit mass then the second term is actually the source term, that is,

$$\left(\frac{\partial \rho}{\partial S}\right)_P = -\frac{\rho}{c_P T} q$$

The equation for conservation of mass then becomes

$$\frac{1}{c^2}\frac{dP}{dt} = -\nabla \cdot (\rho U) + \frac{\rho}{c_P T} q$$

and the conversion to a volume average proceeds by integrating over the surface of the control volume as done in [10]. The main point in the above discussion is that the heat release rate term enters into the equation representing the conservation of mass.

The assumption that is made in this paper is that the heat release rate q is a function of the velocity in the fuel nozzle $q = q(u)$. This modeling assumption has been discussed in detail in [16, 17]. The basis of the assumption is that the unsteady heat release is a function of the equivalence ratio at a flame surface a distance l from the nozzle exit, moreover, the equivalence ratio is only a function of the nozzle exit airflow velocity if the fuel flow is held fixed. The result is that the unsteady heat release $q(t) = f(u(t - l/\bar{u}))$ where $\bar{u}$ is the mean velocity in the nozzle. The main point to be made here is that when a stability boundary is to be computed for the coupled combustion system — the coupling of the acoustics and the unsteady heat release — a feedback loop should exist between the nozzle velocity and the equation for pressure fluctuations in the combustor nozzle.

The form of the feedback can be given more explicitly. The source term F given in equation (1) that represents the effects of combustion is as follows:

$$F(t) = \frac{\rho}{c_p T} q \tag{3}$$

with q being the heat release rate per unit mass. The development in [17] can be used to give a functional form that depends on the nozzle velocity. A modification to the development in [17] is now made. The modeling assumption is that the heat release is split into the mean and fluctuating portions and that the fluctuating component depends only on the fluctuating velocity in the nozzle. Furthermore the heat release model explicitly splits the heat release rate into constant and fluctuating part. This split accounts for the fact that in the thermoacoustic model the coupling of heat release to acoustics in feedback loop occurs through the fluctuating heat release; the corresponding gain parameter for the heat release is then naturally introduced as multiplying the fluctuating portion of the heat release rate. The split between constant and fluctuating heat release rate is given as follows:

$$F(t) = \frac{1}{c_p T}\rho_c A_{nozzle}\bar{u}\overline{\Delta H_s}\left(\bar{\phi} + N\frac{\hat{H}(\phi) - \hat{H}(\bar{\phi})}{\hat{H}(\bar{\phi})}\right) \tag{4}$$

where $\phi = \frac{\bar{\phi}}{1+u'/\bar{u}}$ is the instantaneous equivalence ratio which depends on fluctuating nozzle velocity $u' = u - \bar{u}$ at time $t - \tau$, τ is the convective lag.

In this equation the heat release function $\hat{H}$ is taken from [17] and N is the gain parameter to be used in computing stability characteristics of the model. It is assumed that the mean velocity $\bar{u}$ is equal to the nozzle velocity at steady state conditions, V^s_{nozzle} (see equation (2)) [1]. The steady state conditions refer to the situation when the rate of change of all variables is zero. Figure 4 presents typical time traces for the thermoacoustic model in the instability region. The time traces show the limit cycle behavior captured by the model as the system starts from initial conditions and goes to steady state. Parameter values in (4) are set as $c_p = .24$ $(BTU/\ ^\circ\mathrm{R} - lbm)$, $T = T_4 = 3285$ $(^\circ\mathrm{R})$, $\rho_c = .5807(lbm/ft^3)$, $\overline{\Delta H_s} = 1222$ $(BTU/lbm - mix)$, $\bar{u} = 205.69$ (ft/sec), $A_{nozzle} = 0.0431$ (ft^2).

3 Thermoacoustic Model Analysis: Consequences of Nonlinearities

In this section we analyze the dynamics of the thermoacoustic model. We compute the stability boundary and a few cases showing the dependence of the amplitude of oscillations on parameters of the model. The three varying parameters in the model are N (gain), τ (convective delay) and $\bar{\phi}$ (mean equivalence ratio).

The harmonic balance method combined with parameter continuation (see Appendix) is used to compute the stability diagram and the dependence of amplitude of the limit cycle on model parameters. The $N - \tau$ stability diagram is shown in Figure 5 and it consists of several branches. Only one of them (with lowest frequency) is actually computed; the others are obtained from it by $2\pi k$ (k positive integer) shifts of

[1] Varying $\bar{\phi}$ doesn't change steady state values for any of velocity components but do change all the pressures. Note that when the system is destabilized the unsteady combustion can create mean flow rates that are different from the steady ones because the combusting term F does not generally have zero mean. The nonlinearity takes as input an unsteady fluctuating nozzle velocity with zero mean but will produce as output a fluctuating equivalence ratio with nonzero mean. These effects might be essential when the instability is significant; in this paper, however, the instability is relatively weak and the drift of the dc value with gain can be safely ignored.

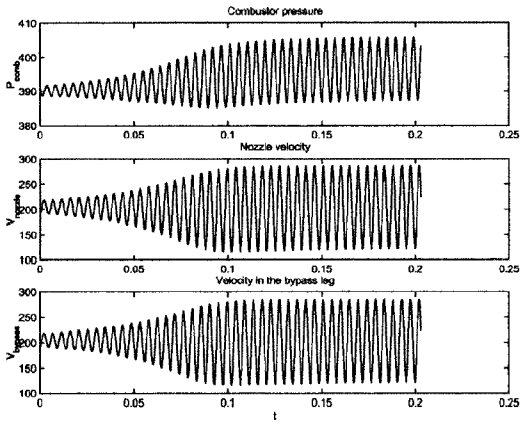

Figure 4: Combustion oscillations in thermoacoustic model at $(N, \tau, \bar{\phi}) = (.25, 3.23, .58)$.

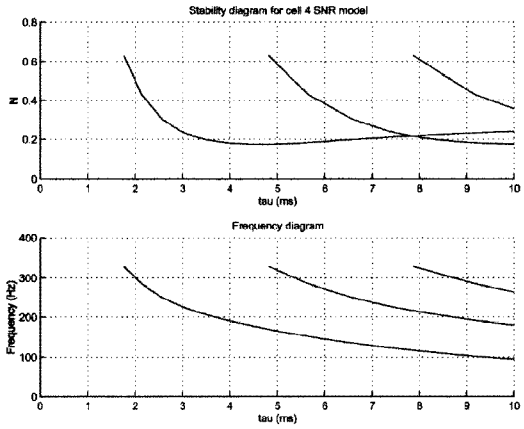

Figure 5: $N - \tau$ stability diagram for thermoacoustic model.

the phase $\omega\tau$ where ω is the frequency. Note that as τ increases ω decreases, which is consistent with a linear stability analysis conducted from a Nyquist diagram of the linearized system. The structure of bifurcation diagram as shown on top panel Figure 5 has certain implications particularly there will be several instabilities encountered as the gain increases. This corresponds to multiple crossings of eigenvalues of the system into the right half of the complex plane which is a consequence of the infinite dimensional nature of the model (delay differential equation). In this paper the focus is on the initial loss of lincar stabilty — the first pair of complex conjugate eigenvalues to cross into the right half plane — and the ensuing limit cycle behavior after this loss of linear stability. The dynamic behavior is known as a Hopf bifurcation.

Figures 6, 7 and 8 present parametric studies of limit cycle regime with varying only one parameter, N, τ and $\bar{\phi}$ respectively. The amplitude diagram is typical for supercritical Hopf bifurcation where the amplitude of oscillation grows smoothly (no jump behavior) after the loss of linear stability.

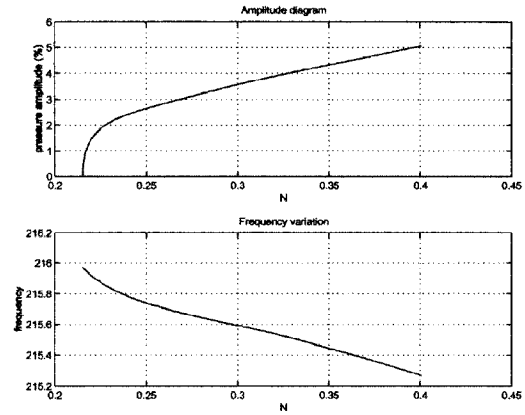

Figure 6: Amplitude diagram with varying gain ($\tau = 3.23, \bar{\phi} = .57$).

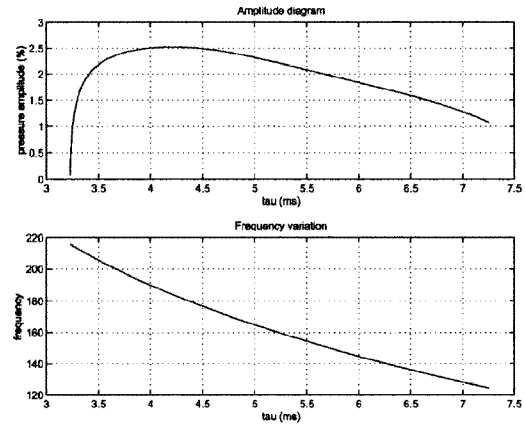

Figure 7: Amplitude diagram with varying delay ($N = .2153, \bar{\phi} = .57$).

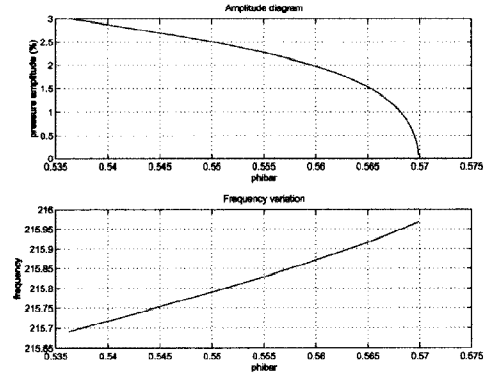

Figure 8: Amplitude diagram with varying mean equivalence ratio ($N = .24, \tau = 3.23$).

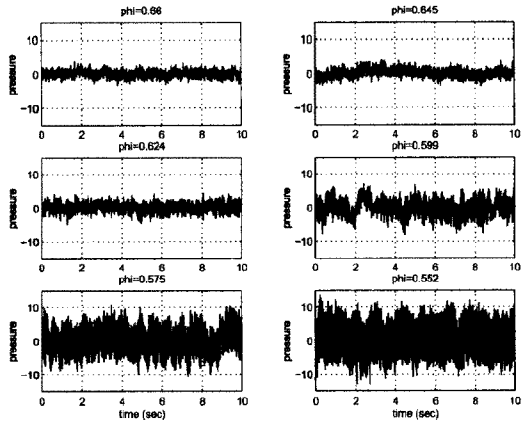

Figure 9: Time traces for the data used for calibration.

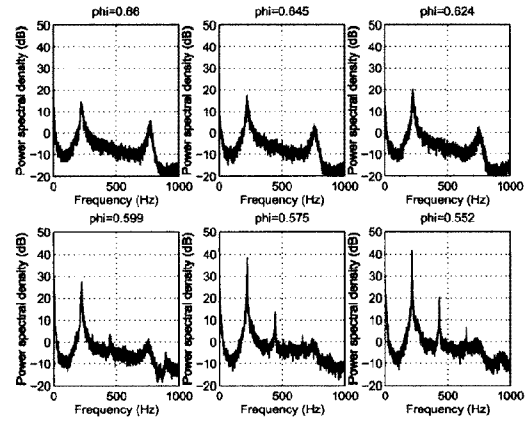

Figure 10: Power Spectral Density for the data used for calibration.

4 Thermoacoustic Model Calibration to Experimental Data

This section describes an approach for model calibration using data obtained in the experimental program. The data used in this section includes five data points with the mean equivalence ratio $\bar{\phi}$ varying between .55 and .66. The magnitude of oscillations reaches 3% at the lowest $\bar{\phi}$, and the frequency varies near 220 Hz. Note that the data are quite noisy so we should make some assumptions in order to interpret the observed behavior as a limit cycle contaminated by noise. The main such assumption is that oscillations in the system are due to the nonlinear mechanism of a feedback coupling of acoustics and heat release (thermoacoustic instability) which leads to the emergence of a limit cycle via a Hopf bifurcation as the equivalence ratio becomes smaller. The equivalence ratio decreases from the top left to the right bottom in the figure. The most important features of Hopf bifurcation, for the purposes of this study, are that the amplitude grows as a square root of the criticality parameter and the frequency varies linearly with the perturbation parameter.

Time traces and power spectral density of pressure signal for chosen data points are shown in Figure 9 and Figure 10. The identified values of the magnitude and (basic) frequency are shown in Figure 11. These qualitatively agree with the Hopf bifurcation scenario, but we notice that the identification procedure we have used produces less reliable results, especially in terms of frequency, for small amplitude oscillations. This may be explained by the low signal to noise ratio. We will consider two approaches to model calibration: one for the original thermoacoustic model where no noise is present and another where noise is included (into the heat release portion) to simulate the effects of turbulence.

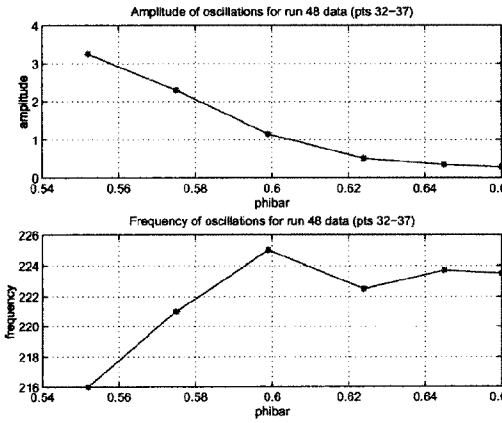

Figure 11: Identified magnitude and frequency of pressure oscillations.

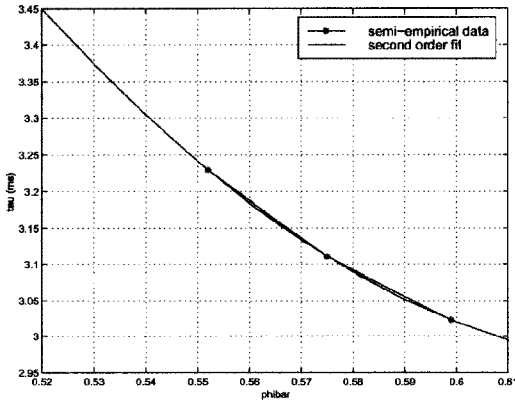

Figure 12: Identified convective delay as a function of equivalence ratio (run 48 data, points 32-34).

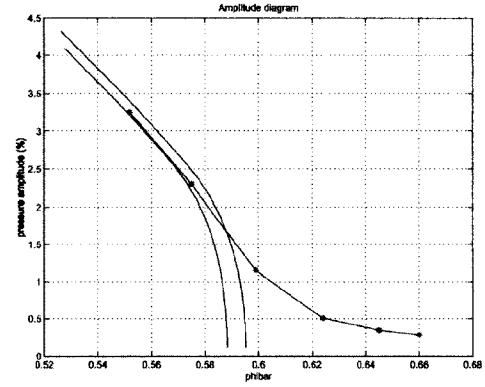

Figure 13: Amplitude dependence on $\bar{\phi}$ for the calibrated model plotted against the experimental data (marked by stars). Three computed curves correspond (from left to right) to $N = .27, .28, .29$.

4.1 Model calibration without noise

The calibration procedure without noise proceeds as follows. We first find a value of the time delay as a function of mean equivalence ratio. The dependence of frequency on the time delay is used to solve the inverse problem: that is knowing the frequency of the limit cycle find the corresponding time delay. The inverse problem can be easily solved graphically or by interpolating data for the stability boundary. It is important to note that the results of this step do not depend on the particular choice of equivalence ratio for which the stability boundary was computed. Using the fact that the frequency of oscillation for available data points is known the corresponding values of time delay can be found. This gives the delay as a function of mean equivalence ratio and a parameterization of this function is found by fitting a second order polynomial. This allows the computation of the dependence of the amplitude of oscillations on $\bar{\phi}$.

The result of applying the outlined procedure to model (1) and experimental data is given in the set of figures described below. Table 3 contains identified values of convective delay. A connection between $\bar{\phi}$ and τ is described by quadratic dependence as illustrated in Figure 12. Using this dependence, amplitude curves have been computed for several values of N; the results and their comparison to the data are shown in Figure 13. The comparison to data indicates that the data fits best with N in the range $.25 - .26$.

4.2 Calibration with noise using statistics of data

It is seen that the pressure data has a large stochastic component that we will refer to as the noise. Especially for the low amplitude oscillations, which occurs the higher mean equivalence ratios, the histogram of the time traces shows a distinctly Gaussian distribution. Therefore, we assume that the system is driven by noise. Note that in [12] effect of addition of noise to a combustion model was studied showing good agreement between the model and data. The noise addition to the model was also supported by results in ([2, 3, 9]). In this work empirical models of single nozzle rig and sector rig operating at high equivalence ratio conditions from forced frequency response experiment were obtained. A stable second order lightly damped system was identified from this experiment. The model was augmented by addition of a white noise input to match the open-loop PSD of the combustor pressure signal. Excellent matches of pressure PSD from the model simulation and from experiment for controlled and uncontrolled system were obtained. A general theory for comparison of models of systems with complex non-equilibrium attractors and stochastically driven systems with applications to model validation and parameter identification is laid out in [14]. This paper also contains an example of parameter identification (delay and noise standard deviation) of a semi-empirical combustion model of the controlled single-nozzle rig operating at high mean equivalence ratio using statistics of data.

In order to deal with this stochastic input explicitly, a random fluctuation is added to the velocity in the nozzle. This random component models turbulence.

If no noise were present, as mentioned earlier in the paper, the equivalence ratio would be $\phi(t) = \bar{\phi}\bar{u}/u(t-\tau)$. The noise is introduced into it in the following manner

$$\phi(t) = \bar{\phi}\bar{u}/\left(u(t-\tau) + N_n\bar{u}r(t)\right) \tag{5}$$

where r is a normally distributed random number with variance 1. The parameter N_n determines the level of input noise entering the system (as a percentage of the mean nozzle velocity).

By comparing statistics of the data with the simulated output of the model, a fit can be done on the model parameters. With noise addition, the parameters of the model are gain N, time delay τ and noise level N_n. Statistics compared are the Power Spectral Density (PSD) and the Probability Density Function (PDF). Since the model can only describe the

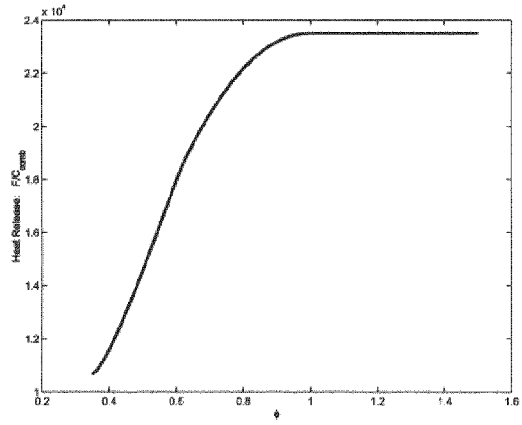

Figure 14: The combined heat release function.

bulk acoustic mode, and the data shows strong component around 750Hz corresponding to a longitudinal mode, the data is filtered around the bulk mode frequency before comparison. Six data sets are available for six different mean equivalence ratios, and for each of these data points, values of these parameters are determined which make the model reproduce the characteristics of the data closely (PSD and PDF). In particular, six values of N and τ, and one N_n are determined. These are shown in Table 4.

Since the heat release rate given by $F(t)$ in equation 4 has N and $\bar{\phi}$ as parameters, this would mean a different function is required to fit the data for every data point. For this reason, a single heat release function was constructed with the help of these six identified functions so that when the model was simulated with it, the model output again matched the data statistics as well as it did with the individual N-dependent functions. Figure 14 shows the heat release function. Figure 15 shows the comparison of PSD and PDF estimates between the data and the model output with this heat release function (N_n and τ values used were the ones given in Table 4). These plots show that the model with the identified heat release function can reproduce the chosen statistics of the data reasonably well. Figure 16 additionally confirms this by showing the comparison of rms as a function of $\bar{\phi}$ from data and the model.

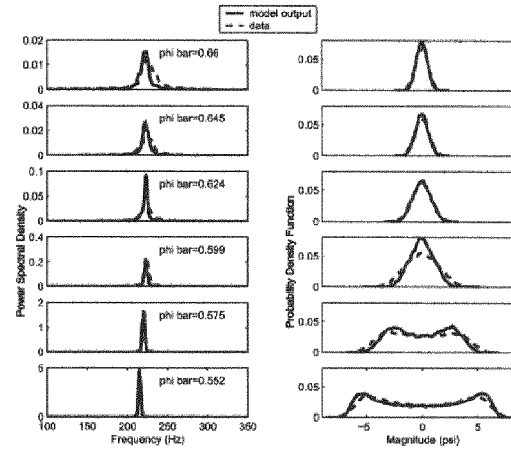

Figure 15: Comparison of data characteristics with that of model output with best-fit heat release function (10% noise). Left column: PSD's; right column: PDF's.

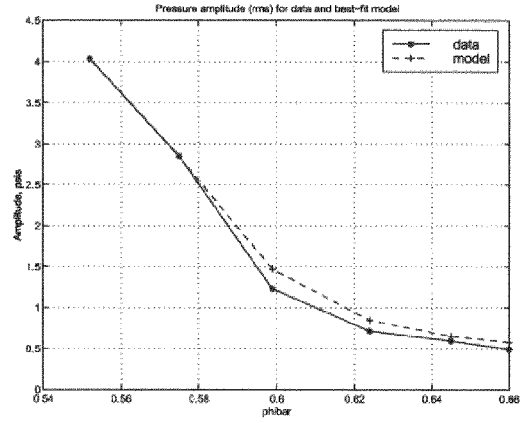

Figure 16: Pressure amplitude (rms) for run 48 data and best-fit model with noise (noise level is the same at all points.)

5 Conclusions

This paper has presented a thermoacoustic modeling framework that describes the results obtained in an experimental program conducted at UTRC.

The paper details the overall modeling approach including the development of physics based acoustics and heat release components. The feedback interconnection of acoustics and heat release — the thermoacoustic model — has been analyzed using a harmonic balance method. This analysis is used to calibrate the model to experimental data, especially, to match amplitudes and frequencies of oscillations seen in

experiments. The matching is accomplished by selection of the empirical portions of the model — the time delay and the heat release gain. The confirmation or match of the model to trends in the amplitude of oscillation as a function of mean equivalence ratio forms the validation of the model.

This paper has developed a methodology for both modeling and analysis that captures experimental data. This methodology consists of the following steps:

1. The development of an acoustic model based on conservation laws. The acoustic model captures the bulk motion in the combustion chamber. The model uses realistic boundary conditions for the premixing nozzle and the exit orifice. The calibration of the acoustic model is done using steady state rig measurements of pressures and mass flow rates and the model predicts the dynamic behavior including acoustic resonance frequencies and damping.

2. The development of a heat release model based mainly on first principles. The heat release model captures the mean heat release as well as the fluctuating component. The fluctuating component is a function of a convective time delay and an empirical gain that both need to be identified from experimental data. The mean heat release is a function of the fuel mass flow rate and equivalence ratio and can be calculated separately.

3. The calibration of the empirical portions of the model to match experimental data. The paper presents two methods for calibration of the model. In the first method the time delay is estimated from experimental data to match the frequency of oscillation and is expressed as a function of mean equivalence ratio. The heat release gain is chosen so that the amplitudes of oscillation of the model matches the experimental data at one value of equivalence ratio. The model is then used to predict the trend of amplitudes with respect to equivalence ratio and this validates the model against experimental data. The validation shows good agreement. In the second method a stochastic fluctuation in the fuel nozzle velocity is introduced and the PSD and PDF properties of the data are matched through adjustment of the noise and gain values. The validation shows better agreement with the data than the first method particularly in the low amplitude portion of the pressure data where the system is expressed as a noise driven stable linear system.

The paper enables a number of subsequent investigations. Some of the immediate ones are as follows:

1. Use of closed loop data for model calibration and validation.

2. Prediction of control authority to match experimental data in a quantitative manner.

3. Use of forced response data to validate the model against experimental data.

4. The calibrated model allows the use of control theory to understand the fundamental limits of controlled performance. This is a standard use of control theory as developed in [18] and applied to combustion processes in [2, 3]. This study of the limits of controlled behavior allows the central parameters to be understood and controllers to be evaluated against absolute metrics and not relative advantages of control design methods.

All of these investigations are expected to increase the fidelity of the model by examining possible deficiencies and through the incorporation of alternate parameter selection or physical mechanisms more accurately describe a wider range of experimental conditions than the open loop matching that is contained in this paper.

Acknowledgments.

The authors wish to acknowledge the overall guidance and program management provided by Drs. Thomas Rosfjord, John McVey, Alan Eckbreth and Richard Murray. The authors also thank Dr. Aldo Peracchio for insightful conversations related to this work. The authors would like to acknowledge significant contribution of Prabir Barooah to calibration of the model with noise. The staff of the Jet Burner Test Stand at UTRC is to be commended for their dedication and professionalism in assisting the authors in obtaining the data that has been used in this paper.

Appendix: Harmonic balance method

The purpose of this appendix is to provide a computational framework, using harmonic balance method, for tracing stability boundaries and tracking periodic orbits as parameters in the model vary. We assume the model to be in the form of differential-delay equation:

$$\dot{x} = F\left(x(t), x(t-\tau), \alpha\right) \tag{6}$$

Here $x \in R^n$ denotes the state vector, τ is the system delay, and α is a scalar parameter.

Let $x = X(t)$ be a periodic solution of the system (6), $X(t+T) = X(t)$, where T is an unknown period. Assuming that $x(t)$ can be approximated by the truncated Fourier series with M harmonics then

$$X_M(t) = x_0 + \sum_{k=1}^{M} \left(p_k \sin(2\pi k\omega t) + q_k \cos(2\pi k\omega t)\right) \tag{7}$$

where $\omega = 1/T$, $x_0, p_k, q_k \in \mathbb{R}^n$. Substituting (7) into (6) and requiring the truncated Fourier series of both sides of (6) be equal yields the following set of M-*th* order harmonic

balance equations:

$$\begin{aligned} F_0 &= 0, \\ FS_k - 2\pi k\omega q_k &= 0, (k = 1, ...M), \\ FC_k + 2\pi k\omega p_k &= 0, (k = 1, ...M), \\ (p_1, q_1) &= 0. \end{aligned} \tag{8}$$

where

$$\begin{aligned} F_0 &= \omega \int_0^{1/\omega} F(X_M(t), X_M(t-\tau), \alpha)dt, \\ FS_k &= 2\omega \int_0^{1/\omega} F(X_M(t), X_M(t-\tau), \alpha)\sin(2\pi k\omega t)dt, \\ FC_k &= 2\omega \int_0^{1/\omega} F(X_M(t), X_M(t-\tau), \alpha)\cos(2\pi k\omega t)dt, \end{aligned} \tag{9}$$

Note that the last equation in (8) fixes the phase thus removing the singularity due to translation invariance of the periodic solution. The algebraic system (8) contains $(2M+1)n+1$ equations and the same number of unknowns (vectors x_0, p_k, q_k, $(k = 1, ...M)$ and frequency ω). Taking τ as another unknown yields a standard continuation problem [1] since the solution set of (8) will generally be a curve. It determines the evolution of a periodic solution as τ varies. Note that instead of τ we may choose α as an active parameter and analyze the dependence of the periodic solution, particularly, its amplitude and frequency, on α.

For the purposes of linear stability analysis linearize equation (6) at the equilibrium point (which is to be determined) and find critical value of delay τ and α such that linearized equation has periodic solutions. Since these solutions are pure harmonics, we use (8) with $M = 1$. We also have to fix the amplitude of oscillations (which because the system is a linear system can be arbitrary, moreover is set by the initial conditions of the defining system of equations) which we do by adding the constraint $(p_1, p_1)(q_1, q_1) - (p_1, q_1)^2 = 1$. In more detail, the defining system for stability calculations is given as follows.

The linearized system (6) at the equilibrium x_0 $(F(x_0, x_0, \alpha) = 0)$ has the form

$$\frac{du(t)}{dt} = Z(x_0, \alpha)u(t) + W(x_0, \alpha)u(t-\tau) \tag{10}$$

where Z and W are $n \times n$ matrices. The defining system now reads:

$$\begin{aligned} F(x_0) &= 0, \\ Zp_1 + NW(p_1\cos(2\pi\omega\tau) + q_1\sin(2\pi\omega\tau)) + 2\pi q_1 &= 0, \\ Zq_1 + NW(-p_1\sin(2\pi\omega\tau) + q_1\cos(2\pi\omega\tau)) - 2\pi p_1 &= 0, \\ (p_1, q_1) &= 0, \\ (p_1, p_1)(q_1, q_1) &= 1 \end{aligned} \tag{11}$$

This system contains $3n+2$ equations and the total number of unknowns (x_0, p_1, q_1, ω) is $3n+1$. Adding τ and α as another unknowns yields a continuation problem for computing the onset of (linear) instability. The projection of the solution curve onto (α, τ) plane defines the α-τ stability diagram. The evolution of frequency along the stability boundary can be seen from projections of the same curve onto (τ, ω) or (α, ω) plane.

We now turn to the problem of computing limit cycles of small amplitude near the stability boundary. Limit cycles near Hopf bifurcation [13] can be approximated with two harmonics $(M = 2)$. The corresponding algebraic system of harmonic balance equations contains $5n + 1$ equations and unknowns. Adding τ (or α) to the set of unknowns yields a continuation problem. The solution of these equations determines the dependence of the amplitude and frequency of oscillations on τ. As we move away from the onset of instability into the unstable region, adding more harmonics might be necessary to represent the limit cycle (particularly when saturation effects of nonlinearity become important) with sufficient accuracy.

References

[1] E.L. Allgower and K. Georg. *Numerical Continuation Methods.* Springer-Verlag, New York, 1990.

[2] A. Banaszuk, C.A. Jacobson, A.I. Khibnik, and P.G. Mehta. Linear and nonlinear analysis of controlled combustion processes. Part I: Linear analysis. In *1999 Conference on Control Applications*, 1999.

[3] A. Banaszuk, C.A. Jacobson, A.I. Khibnik, and P.G. Mehta. Linear and nonlinear analysis of controlled combustion processes. Part II: Nonlinear analysis. In *1999 Conference on Control Applications*, 1999.

[4] J.F. Blackburn, G. Reethof, and J.L. Shearer. *Fluid Power Control.* MIT, Cambridge, MA, 1960.

[5] G.J. Bloxsidge, A.P. Dowling, and P.J. Langhorne. Reheat buzz: an acoustically coupled combustion instability. part 2. theory. *J. Fluid Mechanics*, 193:445–473, 1988.

[6] R. Ernst. Augmentor stability management program. Technical Report AFWAL-TR-2001, Pratt & Whitney, February 1982.

[7] M. Fleifil, A. M. Annaswamy, Z. A. Ghoniem, and A. F. Ghoniem. Response of a laminar premixed flame to flow oscillations: A kinematic model and thermoacoustic instability results. *Combustion and Flame*, 106:487–510, 1996.

[8] J.P. Hathout, A.M. Annaswamy, M. Fleifil, and A.F. Ghoniem. A model-based active control design for thermoacoustic instability. Technical Report 9703, MIT, 1997.

[9] J.R. Hibshman, J.M. Cohen, A. Banaszuk, T.J. Anderson, and H.A. Alholm. Active control of combustion instability in a liquid-fueled combustor. In *1999 ASME Turbo Expo*, 1999.

[10] K.U. Ingard. Analysis of combustor instability. Technical report, UTRC, December 1997.

[11] T. Lieuwen and Ben T. Zinn. The role of unmixedness in driving combustion instabilities in low NOx gas turbines. Technical report, Georgia Institute of Technology, 1999.

[12] T.C. Lieuwen and B.T. Zinn. Investigation of limit cycle oscillations in an unstable gas turbine combustor. In *AIAA Paper 2000–0707, 38th AIAA Aerospace Sciences Meeting*, 2000.

[13] A.I. Mees and L.O. Chua. The Hopf bifurcation theorem and its applications to nonlinear oscillations in circuits and systems. *IEEE Transactions on Circuits and Systems*, CAS–26(4):235–254, April 1979.

[14] I. Mezić and A. Banaszuk. Comparison of complex systems. Submitted to Physica D, 2000.

[15] P.M. Morse and K.U. Ingard. *Theoretical Acoustics*. Princeton University, Princeton, NJ, 1986.

[16] R.M. Murray, C.A. Jacobson, R. Casas, A.I. Khibnik, C.R. Johnson Jr., R. Bitmead, A.A. Peracchio, and W.M. Proscia. System identification for limit cycling systems: A case study for combustion instabilities. In *Proceedings of 1998 American Control Conference*, 1997.

[17] A.A. Peracchio and W. Proscia. Nonlinear heat release/acoustic model for thermoacoustic instability in lean premixed combustors. In *1998 ASME Gas Turbine and Aerospace Congress*. ASME, 1998.

[18] M.M. Seron, J.H. Braslavsky, and G.C. Goodwin. *Fundamental Limitations in Filtering and Control*. Springer, New York, 1997.

Parameter	Description
ρ_3	density at the nozzle exit, (lbm/ft^3)
$L_{nozzle}, L_{perf}, L_{bypass}$	effective nozzle (perforated plate, bypass leg) length, (ft)
$k_{nozzle}, k_{perf}, k_{bypass}$	$1/C_d^2$ for nozzle (perforated plate, bypass leg) flow, (dimensionless)
$V_{nozzle}, V_{perf}, V_{bypass}$	velocity at nozzle (perforated plate, bypass leg) exit, (ft/sec)
$P_{comb}, P_{plenum}, P_{pre}$	pressure in the combustor (plenum, prediffuser), (psia)
$C_{comb}, C_{plenum}, C_{pre}$	capacitance of combustor (plenum, prediffuser) volume, $(ft - sec^2)$
A_e	physical area of exit cross section, (ft^2)
κ	constant in choked flow equation, $(\sqrt{^\circ\mathrm{R}}/\mathrm{sec})$
C_d	discharge coefficient, (dimensionless)
T_4	exit temperature in combustor, (°R)
$\dot{m}_{in}$	upstream mass flow, (lbm/sec)
F	mass flow addition due to heat release(lbm/sec)

Table 1: Description of Model Parameters

Parameter	Value	Comments
ρ_3	.5807	$\mathrm{lbm/ft^3}$
L_{nozzle}	.65	ft
L_{bypass}	.95	ft
L_{perf}	.042	ft
k_{nozzle}	2.0408	dimensionless
k_{bypass}	2.7778	dimensionless
k_{perf}	1.6866	dimensionless
A_{nozzle}	.0431	$\mathrm{ft^2}$
A_{bypass}	.0083	$\mathrm{ft^2}$
A_{perf}	.0313	$\mathrm{ft^2}$
C_{comb}	2.7455×10^{-4}	$\mathrm{ft - sec^2}$
C_{pre}	1.8122×10^{-3}	$\mathrm{ft - sec^2}$
C_{plenum}	4.1853×10^{-3}	$\mathrm{ft - sec^2}$
$\dot{m}_{in}$	6.52	lbm/sec
κ	.532	R/sec
C_d	.98	dimensionless
A_e	.0218	$\mathrm{ft^2}$
T_4	2825+460	° R

Table 2: Parameter Values for Acoustic Portion of Model (1).

Mean equivalence ratio	Amplitude (percent to the mean)	Frequency (Hz)	Identified delay (ms)
0.5520	3.25	216	3.23
0.5750	2.3	221	3.11
0.5990	1.149	225	3.02
0.6240	0.5075	222	N/A
0.6450	0.3410	223.7	N/A
0.6600	0.2795	223.5	N/A

Table 3: Data from run 48 and identified value of delay

Mean equivalence ratio	Best-fit N	Best-fit τ (ms)	N_n (noise level)
0.66	0.278	3.0	0.1
0.645	0.272	3.0	0.1
0.624	0.259	3.0	0.1
0.599	0.244	3.0	0.1
0.575	0.22	3.08	0.1
0.552	0.19	3.20	0.1

Table 4: Best fit values of N, τ and N_n to data from run 48.

PAPER -30, C. Jacobson

Question (M. Huth, Germany)

How can models developed for a single burner test rig be used in an annular combustion arrangement? How are the circumferential modes described?

Reply

The UTRC approach has been to develop combustion dynamics models by reducing the number of fuel injectors, but keeping the environment (pressure, temperature) realistic relative to the engine operating conditions. Hence the heat release models are realistic and the acoustic model may be changed to model different situations (longitudinal, tangential modes).

Question (S. Candel, France)

Can you explain the meaning of the gain parameter and is this gain parameter a function of frequency? Also, in many cases the response of a confined flame is strongest in regions where the gain of the transfer function is not very large but where the phase is large.

Reply

The dynamic model developed uses physics-based models. However, these models were very simplified. In the procedure described in the paper, a free parameter ("gain") is interested to capture some neglected heat release characteristics. This gain parameter is expected to be O(1) if the model is accurate (which it was found to be when N $\approx$ 0.2 in the calibration procedure).

The heat release model was derived based on the work of Proscia and Peracchio. In this model, both equivalence ratio and flame sheet dynamics are considered and, in this full model, there will be a frequency dependence (because of the flame sheet dynamics). This dependence was not found to be significant for the behavior being captured by the model and hence was deleted to have the simplest model available.